







Spectroscopy of adiabatic dark states under two-photon excitation of sodium atoms

Arturs Cinins¹, Milan S. Dimitrijević^{2,3}, Vladimir A. Srećković⁴,
Martins Bruvelis⁵, Kaspars Miculis^{1,6}, Nikolai N. Bezuglov^{7,8} and
Aigars Ekers⁵

¹ *Institute of Atomic Physics and Spectroscopy, University of Latvia, LV-1004 Riga, Latvia, (E-mail: arturs.cinins@lu.lv)*

² *Astronomical Observatory, Volgina 7, 11060 Belgrade, Serbia, (E-mail: mdimitrijevic@aob.rs)*

³ *LERMA, Observatoire de Paris, Université PSL, CNRS, Sorbonne Université, F-92190 Meudon, France*

⁴ *Institute of physics Belgrade, University of Belgrade, P.O. Box 57, Belgrade, 11001, Serbia, (E-mail: vlada@ipb.ac.rs)*

⁵ *King Abdullah University of Science and Technology (KAUST), Computer, Electrical and Mathematical Sciences and Engineering Division (CEMSE), Thuwal 23955-6900, Saudi Arabia, (E-mail: martins.bruvelis@gmail.com)*

⁶ *National Research Nuclear University MEPhI, Moscow, 115409 Russia, (E-mail: kaspars.miculis2@lu.lv)*

⁷ *Sankt-Petersburg State University, 199034 St. Petersburg, Russia, (E-mail: nikolay.bezuglov@gmail.com)*

⁸ *Rzhanov Institute of Semiconductor Physics SB RAS, Novosibirsk, Russia*

Received: September 23, 2023; Accepted: October 22, 2023

Abstract. This work focuses on visualization of dark states arising in systems of hyperfine states upon two-photon excitation. In our experiment, levels $3S_{1/2}$ and $3P_{1/2}$ of sodium atoms are coupled by a strong S-laser field forming the laser-dressed adiabatic states, which are then monitored by scanning a weak probe P-field across the $3P_{1/2} \rightarrow 7D_{3/2}$ transition. The excitation spectrum of the $7D_{3/2}$ state exhibits one main peak and several side peaks. The latter shift farther apart with increasing S-laser intensity, while the position of the main peak is hardly affected, which associates its origin with a class of dark states decoupled from laser interactions. The results of numerical simulation of the observed spectra based on the solution of the optical Bloch equations are in good agreement with the experimental data. The results are of interest for atomic and laser physics.

Key words: laser excitation – optical adiabatic states – Na spectra – dark state peaks

1. Introduction

Adiabatic processes are observed in many fundamental and applied issues of natural science, having a wide range of applications depending on the characteristics of the problems. The quantum-mechanical theory has added its own specific approaches to the traditional methods of studying adiabatic phenomena in the classical sections of physical kinetics of gaseous geo- and space media (including plasma). These approaches include the formalism of adiabatic states, introduced as eigenfunctions ψ_κ

$$\hat{H}(I)\psi_\kappa(I) = \varepsilon_\kappa(I)\psi_\kappa(I) \quad (1)$$

of a non-stationary Hamiltonian $\hat{H}(I)$, which depends on slowly varying external parameters $I(t)$ (Landau, Lifshitz, 1981; Schiff, 1968). When studying dynamics of atomic or molecular formations, the parameters I are represented by internuclear distances R (Nikitin, Umanskii, 1984).

In contemporary problems of controlling atomic/molecular multilevel systems, the particles are subjected to optical coupling by pulsed laser fields. For quasi-resonant dipole transitions between energy levels, the field amplitudes are conventionally incorporated into the so-called Rabi frequencies $\Omega(t)$ (Shore, 2017). The corresponding adiabatic states ψ_κ (termed laser-dressed states in quantum optics (Shore, 2017; Vitanov *et al.*, 2017), with Rabi frequencies Ω as parameters I are classified into three categories - Dark, Bright, and Chameleon states (Shore, 2017; Kirova *et al.*, 2017). Dark states are completely decoupled from the laser-atomic interaction. Therefore, they do not directly contribute to the fluorescence spectra, while their adiabatic “dark” energies $\varepsilon_\kappa^{(D)}$ (AC Stark shifts) are inherently insensitive to changes in Ω . Bright states, on the contrary, are responsible for the interaction with laser fields and, therefore, participate in the absorption spectra formation, while the associated adiabatic “bright” energies $\varepsilon_\kappa^{(Br)}$ experience strong Stark shifts. Chameleon states are endowed with the properties of both dark states, due to the fact that they are not directly involved in the excitation of the atomic system (Kirova *et al.*, 2017), and bright states, since their energies also significantly depend on Rabi frequencies (Cinins *et al.*, 2022 a).

Noteworthy, the dark states emerge from a coherent mixture of stable sub-levels (belonging to HF or Zeeman structures) of the system ground state, i.e. they turn out to be little susceptible to various dephasing effects that are inherent in excited states due to the processes of radiative decay or strong interatomic interaction (Van Der Waals, dipole-dipole, etc.). For this reason the dark states are widely used in quantum optics for design and subsequent practical implementations of new phenomena or quantum formations (such as electromagnetically induced transparency (Fleischhauer *et al.*, 2005) or polaritons - a coherent composition of photonic and atomic states (Fleischhauer, Juzeliūnas, 2016), as well as to find highly efficient algorithms for performing quantum operations based on adiabatic passage processes (Rousseaux *et al.*, 2013; Cinins

et al., 2022 b). In this context, real-time monitoring and control of the evolution of dark states presents a challenging practical task. Here we present an experimental scheme for optical diagnostics of dark states, based on the non-trivial possibility of their manifestation in absorption spectra upon two-photon excitation of sodium atoms.

In what follows, the principal quantum numbers and the orbital, electronic, and total angular momenta of atoms are denoted by n , L , J , and F , respectively.

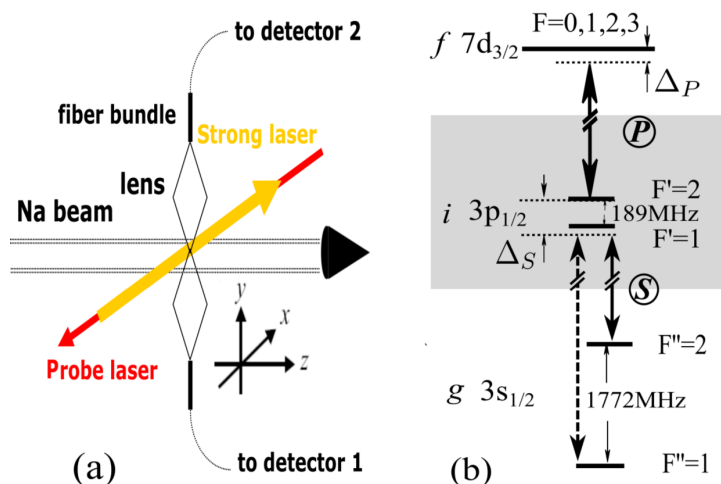


Figure 1. (a) Geometry of the experiment with a supersonic beam of Na atoms and (b) the corresponding ladder excitation scheme. The two S- and P-laser beams counter propagate along the x -axis. The lasers linear polarization vectors and the atomic beam axis are parallel to the z axis, which is also chosen as the quantization axis.

2. Experiment

2.1. Experimental setup

The experiment was performed in a supersonic beam of Na atoms with a mean flow velocity $v_f = 1160$ m/s. Two skimmers and a 2-mm entrance aperture of the excitation zone colimate the beam to the divergence angle of $0.67^\circ \pm 0.02^\circ$, which corresponds to the residual FWHM Doppler widths of 11.2 MHz and 14.7 MHz for one-photon excitation wavelengths of 589 and 450 nm, respectively.

The Na atoms are excited and probed upon crossing at a right angle two mutually collinear, anti-parallel laser beams S and P (see Fig. 1 (a)). The strong S-laser beam from a single-mode Coherent CR-699-21 ring dye laser couples a hyperfine component of sodium D_1 line at 589.5 nm, and the weaker probe P-laser beam from a TOPTICA TA-SHG 110 semiconductor laser couples the

second transition between $3p_{1/2}$ and $7d_{3/2}$ near 449.4 nm. Both lasers have narrow line with below 1 Mhz, and they are linearly polarized in the direction \mathbf{e}_z of the atomic beam axis z , which serves as the quantization axis. The number density of atoms in the laser excitation region was chosen sufficiently low ($\leq 10^{10}\text{cm}^{-3}$), ensuring that the effects of radiation trapping and reabsorption (Bezuglov *et al.*, 2003) can be safely neglected.

The two-photon excitation $3s_{1/2}, F'' \rightarrow 3p_{1/2} \rightarrow 7d_{3/2}$ of Na shown in Fig. 1 (b) implies a two-step process. At the first step, the S-laser (strong laser) provides strong coupling of Zeeman sublevels M'' from one of the ground hyperfine (HF) g -component F'' and F' , M' -sublevels of the first excited (intermediate) i -state $3p_{1/2}$. The laser-dressed (adiabatic) states, arising in the strongly coupled multilevel $g-i$ system, are probed by weak coupling by P-laser to the final excited f -state $7d_{3/2}$. Detunings $\Delta_{P,S}$ of the laser fields with frequencies $\omega_{P,S}$ are defined relative to the resonance (Bohr) frequencies of the respective HF transitions between components with $F'' = 1, 2$ and $F' = 2$ in the case of S-laser, and between $F' = 2$ and $F = 2$ for P-laser. The linear polarizations of both lasers imply that the total atomic angular momentum projection is conserved in both transitions, i.e. $\Delta M_{g \rightarrow i, i \rightarrow f} = 0$.

The fluorescence emitted by Na atoms is collected by lenses into two fiber bundles at a right angles with respect to both atom beam and laser beams axes. The collected light is then guided via spectral filters into two photomultipliers. Photocurrent signals are accumulated using a SRS SR400 photon counter. We record the total fluorescence from the level f (by detector 2) as a function of the P-laser detuning Δ_P for a fixed S-laser detuning Δ_S and refer to this signal as a spectral profile. In addition, auxiliary detector 1 registers photons emitted by the i -levels. Both signals are proportional to the integral (over excitation volume and HF sublevels) populations of the respective excited states.

2.2. Experimental parameters

The use of counterpropagating laser beams in the ladder excitation scheme corresponds to a typical Doppler-free setting of the experiment in atomic-molecular spectroscopy (Vitanov *et al.*, 2017; Bruvelis *et al.*, 2012). The P,S-beams are focused using cylindrical lenses such that the long axis of the focus is perpendicular to the atomic beam axis. The chosen here typical in our experiments beam waists $\varpi_S = 20.5\mu\text{m}$ of the S- (strong) and $\varpi_P = 70\mu\text{m}$ of the P- (probe) laser beams allows safely ignoring the effects of laser wave-front curvatures (Bruvelis *et al.*, 2012). The relatively small waist of strong S-laser reduces the effects of optical pumping (Sydoryk *et al.*, 2008; Porfido *et al.*, 2015).

The laser spatial intensity profiles are Gaussian and along z -axis is $I_j(z) \sim \exp(-z^2/\varpi_j^2)$ ($j = P, S$). The mean flow velocity v_f of atoms is 1160 m/s, so that the transit times (Sydoryk *et al.*, 2008) $\tau_j = 2\varpi_j/v_f$ of atoms through the laser beams are $\tau_S = 37\text{ns}$ and $\tau_P = 126\text{ns}$ for S- and P-lasers respectively. The above distributions $I_j(z)$ result in the Gaussian time variations

$$I_j(t) = I_j^{(0)} \exp(-4t^2/\tau_j^2); \quad j = P, S \quad (2)$$

of laser intensities in the moving frame of an atom ($t = z/v_f$).

In the rotating-wave approximation (RWA) (Shore, 2011), the atom-light interaction is determined by slowly varying vector amplitudes $\mathbf{E}_j(t) \sim \sqrt{I_j(t)}$ of the laser electric fields. The corresponding field operators $\hat{V}_j = -0.5\hat{\mathbf{d}}\mathbf{E}_j$ describe the coupling of the atomic electric dipole moment $\hat{\mathbf{d}}$ with P - and S -laser fields $\mathbf{E}_j = E_j\mathbf{e}_z$ linearly polarized along the quantization axis z , that is

$$\hat{V}_{S,P}(t) = -0.5\hat{d}_z E_{S,P}(t) \quad (3)$$

It is convenient to describe the laser induced couplings using the characteristic Rabi frequencies $\Omega_{P,S}$ (the so called reduced Rabi frequencies) that drive the transitions $3s-3p$ and $3p-7d$ (Sydoryk *et al.*, 2008):

$$\begin{aligned} \Omega_S &= E_S(z=0) \cdot |(3s \parallel D \parallel 3p)|/\hbar; \\ \Omega_P &= E_P(z=0) \cdot |(3p \parallel D \parallel 7d)|/\hbar. \end{aligned} \quad (4)$$

Here $(\tilde{n}l \parallel D \parallel nl)$ are the corresponding reduced matrix elements for the discussed transitions, considered unresolved with respect to fine and hyperfine structure (Sobelman, 1992).

Equation (4) defines the reduced Rabi frequencies Ω_j via maximum values $E_j^{(0)} \equiv E_j(z=0)$ of the laser electrical field amplitudes at the center parts $z = 0$ of the laser beams. Practically more convenient is the relation (Sydoryk *et al.*, 2008; Metcalf, van der Straten, 1999):

$$\Omega_j^2 = g_j A_j \frac{3\lambda_j^3}{4\pi^2\hbar c} I_j^{(0)}; \quad W_j = \pi I_j^{(0)} \varpi_j^2 \quad (5)$$

between the reduced frequencies Ω_j and intensities $I_j^{(0)}$ entering Eq. (2) which are easily found from the measured laser powers W_j . Here λ_j and A_j are the wavelength and the Einstein coefficient of the j -transition $\tilde{n}l - nl$, and $g_j = 2l+1$ is the the statistical weight of the transition upper level nl .

3. Results and discussion

The fluorescence signal S_f observed in the experiment is proportional to the integral population \bar{n}_f of the final $7d_{3/2}$ state of an atom. This population can be found in terms of the total number of photons N_f emitted by the corresponding HF and Zeeman components F, M having the partial populations $n_{FM}^{(f)}(t)$ at the time t in the moving frame of an atom:

$$S_f \sim N_f = A_f \bar{n}_f; \quad \bar{n}_f = \int_{-\infty}^{\infty} \sum_{FM} n_{FM}^{(f)}(t) dt, \quad (6)$$

where A_f is a natural width of the f-state.

3.1. Numerical modeling

For obtaining the emitted photon number N_f one should solve the modified Optical Bloch equations (Shore, 2011)

$$\frac{d\rho}{dt} = -i [\hat{H}\rho] + \hat{R}\rho. \quad (7)$$

for atomic density matrix ρ of the sodium atoms ensemble under study. The total Hamiltonian \hat{H} of the atom-laser system in RWA

$$\hat{H}_{RW} = \hat{H}^{(a)} + \hat{H}^{(hf)} + \hat{V}_S(t) + \hat{V}_P(t) \quad (8)$$

describes interaction of Na atoms with external electromagnetic fields. The atomic Hamiltonian $\hat{H}^{(a)}$ that includes the fine structure interaction along with the HF operator $\hat{H}^{(hf)}$ give the energy structure of the diabatic (bare) states of isolated atoms. The field operators $\hat{V}_{S,V}$ (3) are responsible for the laser-atom interaction which is depicted in Figs. 1(b). The term \hat{R} deals with relaxation processes caused by spontaneous emission and the finite laser linewidths. The diagonal elements $\rho_{\kappa,\kappa}$ of the matrix ρ give the population n_κ of quantum state $|\kappa\rangle$, while the off-diagonal elements $\rho_{\kappa,\kappa'}$ belong to the so-called coherences.

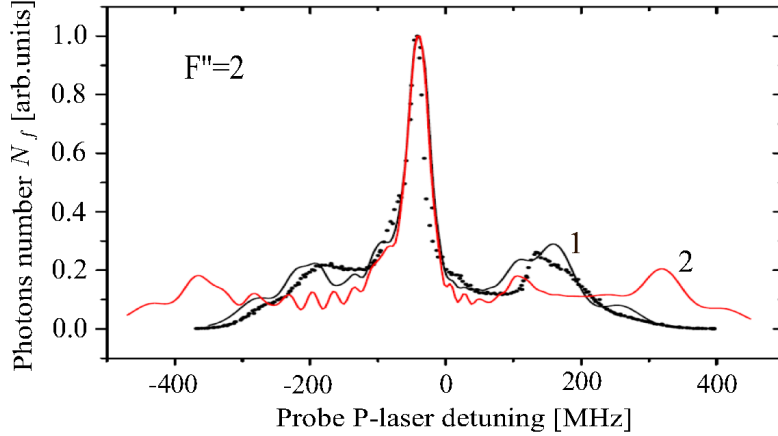


Figure 2. The total number N_f of photons emitted by the final $7d_{3/2}$ state of Na atoms vs probe P-laser detuning Δ_P for the $3s_{1/2}(F'' = 2) \rightarrow 3p_{1/2} \rightarrow 4d_{3/2}$ excitation sequences with HF ground state component $F'' = 2$. The experimental (dot curve) and the theoretical (solid curve 1) profiles correspond to S-laser reduced Rabi frequency (4) $\Omega_S = 1200\text{MHz}$ while theoretical profile 2 (red solid curve) is calculated for $\Omega_S = 2000\text{MHz}$. The probe P-laser reduced Rabi frequency (4) $\Omega_P = 7\text{MHz}$. The strong S-laser detuning $\Delta_S = -120\text{MHz}$.

Matrix elements of the field operators describe a variety of stimulated transitions among the HF and Zeeman sublevels. The absolute strengths of the transitions are connected with the reduced Rabi frequencies (4). Rabi frequencies of individual fine $LJ \rightarrow \tilde{L}\tilde{J}$ and HF $LJF \rightarrow \tilde{L}\tilde{J}\tilde{F}$ transitions are then defined by the tabulated line strength values (Sobelman, 1992). The Rabi frequencies for individual transitions $LJFM \rightarrow \tilde{L}\tilde{J}\tilde{F}\tilde{M}$ between Zeeman sublevels M in the case of linearly polarized excitation are obtained using the formulas provided in (Sobelman, 1992; Auzinsh *et al.*, 2010), and the respective values can be found in (Sydoryk *et al.*, 2008; Bruvelis *et al.*, 2012).

Here we employ a numerical algorithm akin to our previous works (Cinins *et al.*, 2022a; Sydoryk *et al.*, 2008; Bruvelis *et al.*, 2012), i.e. an algorithm based on the split operator technique. The latter has increased stability of symplectic numerical integration schemes (Hairer *et al.*, 2006) and is successfully used to solve a wide range of problems in the theory of radiation transfer in dense absorbing media (Kazansky *et al.*, 2001), laser spectroscopy (Kirova *et al.*, 2017), and in the analysis of the dynamic chaos regime in Hamiltonian systems (Efimov *et al.*, 2014).

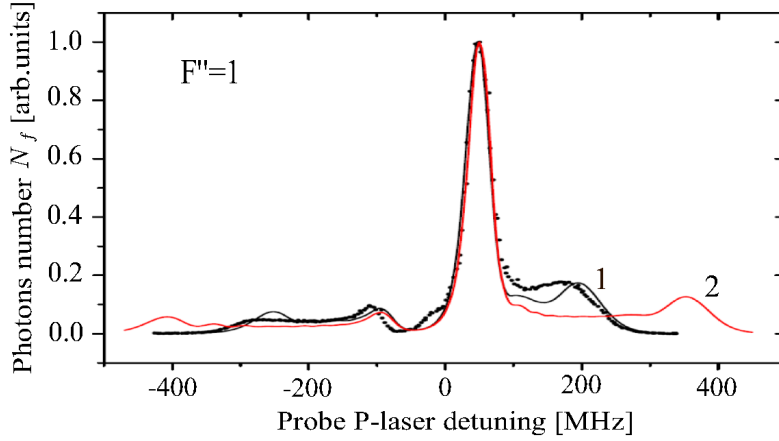


Figure 3. The same as in Fig. 2 in the case of the the initially populated HF component $F'' = 1$ and the strong S-laser detuning $\Delta_S = -178\text{MHz}$.

3.2. Experimental and numerical results

Figures 2 and 3 show excitation fluorescence from the upper f-level as a function of the S-laser detuning Δ_S for several values of both P-laser detuning Δ_P and the initially populated HF component F'' of the ground $3s_{1/2}$ state. The circles correspond to experimental values and the solid lines are results of numerical calculations discussed above. In the following subsections, we will provide a detailed interpretation of the obtained spectra.

3.3. Discussion

Upon coupling with linearly polarized photons, the atomic magnetic (Zeeman) quantum number M is an exact invariant (Landau, Lifshitz, 1981), i.e. atomic system in Fig. 1(b) is decomposed into a set of independent (mutually orthogonal) partial excitation ladders (M-ladders) whose levels are labeled only by the HF quantum numbers F , as shown in Fig. 4(a).

Qualitative interpretation of the excitation spectra exhibited in Figs. 2-3 is based on the concept of adiabatic (dressed) states for strongly coupled sub-levels of (g-i) system. Let us first introduce a somewhat idealized atomic model to provide an illustrative explanation of the observed spectra features, in particular, the existence of central peaks without any noticeable influence of the S-laser intensity on them. We accept the following two main simplifications. (i) All atoms move at the same flow velocity v_f (i.e. one disregards Doppler broadening); (ii) The HF splitting between the HF components $F' = 1, 2$ of $3p_{1/2}$ i-state can be neglected in the first approximation (the final state $7d_{3/2}$ fully meets this requirement). The second assumption means that the partial simplified excitation ladders have a non-degenerate lower state (F''), a doubly degenerate i-state ($F' = 1, 2$), and a triply degenerate f-state (due to the selection rule $\Delta F = 0, \pm$).

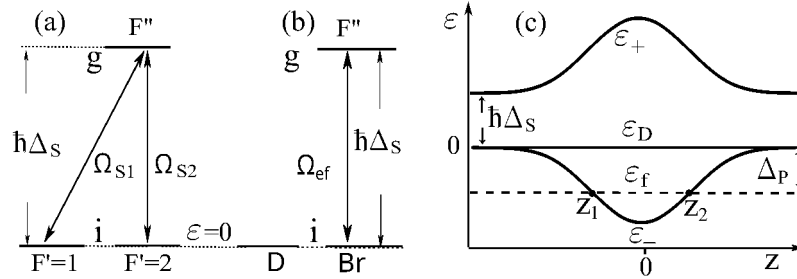


Figure 4. (a) The first (g-i) excitation step with some fixed value of Zeeman quantum number M under the rotating-wave approximation (RWA) and in neglecting the HF interaction for the $3p_{1/2}$ i-state. (b) The same excitation scheme as in frame (a) in the Dark-Bright basis. (c) Atomic energy level diagram of laser-dressed states with beam axis coordinate $z = v_f \cdot t$ as a parameter. The excitation of the final f-state $7d_{3/2}$ occurs at the intersection (Landau-Zener) points $z_{1,2}$.

The main features of fluoresce signals are determined by the atomic adiabatic (dressed) states ψ_κ (more precisely, by their energies ε_κ) formed by strong S-laser at the first excitation step shown in Fig. 4(a) for M-ladder. This step turns out to be a conventional Lambda-excitation scheme with the following parameters. We choose as zero the atomic energy ε of the diabatic HF component $\psi_{F'1} \equiv |iF' = 2\rangle$ of $3p_{1/2}$ i-state, i.e. under the simplified model $\varepsilon_{F'=1,2} = 0$. In RWA, the

diabatic energies of g-,f-states are defined by the corresponding laser detunings: $\varepsilon_{F''} = \hbar\Delta_S$ and $\varepsilon_F = -\hbar\Delta_P$ as seen in Fig. 4(a). The partial Rabi frequencies $\Omega_{S1,2}$ are proportional to the reduced S-frequency Ω_S (4) with coefficients of proportionality ~ 0.2 depending on the quantum numbers M, F'', F' via 6j- and 3j-symbols (Sydoryk *et al.*, 2008; Sobelman, 1992).

The algorithm for obtaining the adiabatic states ψ_κ for Lambda-schemes is well known and includes two sequential actions (Vitanov *et al.*, 2017; Shore, 2011; Cinins *et al.*, 2023). (i) First, two new mutually orthogonal wave vectors ψ_D and ψ_{Br} are constructed

$$\psi_D = \frac{\Omega_{S1}}{\Omega_{ef}}\psi_{F'2} - \frac{\Omega_{S2}}{\Omega_{ef}}\psi_{F'1}; \quad \psi_{Br} = \frac{\Omega_{S2}}{\Omega_{S1}}\psi_{F'1} + \frac{\Omega_{S1}}{\Omega_{ef}}\psi_{F'2}; \quad \Omega_{ef} = \sqrt{\Omega_{S1}^2 + \Omega_{S2}^2}. \quad (9)$$

Vectors $\psi_{D,Br}$ differently relate to the RWA g-sublevels $\psi_{F''} \equiv |gF''\rangle$: completely decoupled *D*-vector ψ_D (termed "Dark") and *Br*-vector ψ_{Br} (termed "Bright") with coupling Rabi frequency Ω_{ef} (see Fig. 4(b)). (ii) Second, linear combination of a coupled pair of diabatic vectors $\psi_{Br}, \psi_{F''}$ provides two new adiabatic states (eigenstates) ψ_\pm

$$\psi_+ = \cos\theta\psi_{F''} + \sin\theta\psi_{Br}; \quad \psi_- = -\sin\theta\psi_{F''} + \cos\theta\psi_{Br}, \quad (10)$$

with newly acquired repulsive adiabatic energies

$$\varepsilon_\pm(z) = \frac{\hbar}{2}\Delta_S \pm \frac{\hbar}{2}\sqrt{\Delta_S^2 + \Omega_{ef}(z)^2}; \quad z = v_f \cdot t, \quad (11)$$

due to ac Stark shift (Delone, Krainov, 1999) stimulated by the coupling frequency Ω_{ef} (9). The mixing angle $2\theta = \arctan(-2\Omega_{ef}/\Delta_S)$ ($0 \leq \theta \leq \pi/2$) in Eq. (10) defines a measure of amplitudes sharing between the diabatic vectors $\psi_{F''}, \psi_{Br}$.

Importantly, in the moving frame of the atom the Rabi frequencies $\Omega_j(z)$

$$\Omega_j \rightarrow \Omega_j(z) = \Omega_j(z=0) \cdot \exp(-z^2/2\varpi_j^2); \quad (12)$$

along with ac Stark shifts ε_\pm (9) become z- and time-dependent (see Fig. 4(c)). The energy ε_D of the dark state, on the contrary, since it is not involved into the light-atom interaction, always remains equal to diabatic zero value $\varepsilon_D = 0$, as depicted in Fig. 4(c).

Probing the spatially varying energies $\varepsilon_\pm, \varepsilon_D$ of the dressed adiabatic states at the second stage of the ladder scheme using a weak P-probe laser has a number of interesting features. Due to the different spatial behavior of ε_\pm and ε_D , the bright and dark states are responsible for the formation of different parts of the N_f (6) fluorescence signal as a function on P-laser detuning Δ_P .

(i) In the case of ψ_\pm vectors, they coherently share the population with the ground state $\psi_{F''}$ (see Eq. (10)) and can transfer it to f-states only at two

Landau-Zener resonance points $z_{1,2}$, shown in Fig. 4(c). The maximum probability of population transfer occurs at point $z=0$, i.e. the intersections of the horizontal lines $\varepsilon = \hbar\Delta_P$ with curves $\varepsilon = \varepsilon_{\pm}$ provides a wide fluorescence signal background with width $\Delta\omega_f \approx (\varepsilon_+ + |\varepsilon_-|) \sim \Omega_S$. These findings of ours correlate well with the data presented in Fig. 2,3.

(ii) The dark state ψ_D (9), completely decoupled from the laser-atom interaction, cannot be excited by the S-laser and, at first glance, does not contribute to the N_f signal. There is, however, another way of its excitation, namely due to HF splitting $\Delta_{HF} = 189\text{MHz}$ between $F' = 1$ and $F' = 2$ HF components of $3p_{1/2}$ i-state. As mentioned in (Shore, 2017; Vitanov *et al.*, 2017; Auzinsh *et al.*, 2008), the splitting Δ_{HF} , often called the double-photon detuning, opens a pathway for population flow from ψ_{Br} to ψ_D states. Since the potential curves $\varepsilon_{D,f}$ of D- and f-states intersect in our simplified model only at $\Delta_P = 0$, the D-state manifests itself in the $N_f(\Delta_P)$ signal as a central peak blurred and shifted from resonance $\Delta_P = 0$ by HF interaction. The characteristics of this "Dark" peak, determined solely by Δ_{HF} , should be slightly affected by the intensity of the S-laser, which is consistent with the spectral profiles in Fig. 2,3.

4. Conclusions

In this work, the processes of formation of laser-dressed states on the hyperfine (HF) sublevels of sodium atoms are experimentally and theoretically studied using two-photon laser spectroscopy. A supersonic beam of sodium atoms is excited near the frequency of the D_1 line by a strong S-laser, which induces formation of a system of bright and dark adiabatic states from the HF components of the $3p_{1/2}$ state. Probing the $3p_{1/2} \rightarrow 7d_{3/2}$ transition with a weak P-laser allows to diagnose the dressed state parameters based on the features of the $7d_{3/2}$ state emission spectrum. Numerical calculations, which describe well the experimental data, followed by their qualitative analysis, made it possible to explain the presence of two characteristic structural parts of the spectra. The first of them, which has a large spectral extent with a width proportional to the S-laser intensity, is formed by bright states since the associated adiabatic energies alter along the atomic beam axis in the laser excitation zone. The second region, presented in the spectra as a relatively narrow central peak, weakly responds to the excitation intensity and, as analysis shows, is formed by transferring the population of the bright state to the dark one due to their mixing by the HF interaction operator. Thus, we have proposed and implemented an experimental scheme for optical diagnostics of dark states, based on their visualization in two-photon absorption spectra of sodium atoms. The results are of interest for atomic and laser physics.

References

- Auzinsh, M., Bezuglov, N.N., Miculis, K.: 2008, *Phys. Rev. A*, **78**, 053415
- Auzinsh, M., Budker, D., Rochester, S.: 2010, *Optically Polarized Atoms: Understanding Light-atom Interactions*, OUP Oxford
- Bezuglov, N.N., Ekers, A., Kaufmann, O., Bergmann, K., Fuso, F., Allegrini, M.: 2003, *Journal of Chemical Physics*, **119**, 7094
- Bruvelis, M., Ulmanis, J., Bezuglov, N.N., Miculis, K., Andreeva, C., Mahrov, B., Tretyakov, D., Ekers, A.: 2012, *Phys. Rev. A*, **86**, 012501
- Cinins, A., Bruvelis, M., Bezuglov, N.N.: 2022 a, *Journal of Physics B: Atomic, Molecular and Optical Physics*, **55**, 234003
- Cinins, A., Bruvelis, M., Dimitrijević, M.S., Srećković, V.A., Efimov, D.K., Miculis, K., Bezuglov, N.N., Ekers, A.: 2022 b, *Astronomische Nachrichten*, **343**, e210081
- Cinins, A., Dimitrijević, M.S., Srećković, V.A., Miculis, K., Bezuglov, N.N.: 2023, *The European Physical Journal D*, **77**, 87
- Delone, N.B., Krainov, V.P.: 1999, *Physics-Uspekhi*, **42**, 669
- Efimov, D.K., Bezuglov, N.N., Klyucharev, A.N., Gnedin, Y.N., Miculis, K., Ekers, A.: 2014, *Optics and Spectroscopy*, **117**, 8
- Fleischhauer, M., Imamoglu, A., Marangos, J.P.: 2005, *Rev. Mod. Phys.*, **77**, 633
- Fleischhauer, M., Juzeliūnas, G.: 2016, Slow, stored and stationary light, in: *Optics in Our Time*, 359
- Hairer, E., Wanner, G., Lubich, C.: 2006, *Geometric Numerical Integration: Structure-Preserving Algorithms for Ordinary Differential Equations*, Springer Berlin Heidelberg: Berlin, Heidelberg
- Kazansky, A.K., Bezuglov, N.N., Molisch, A.F., Fuso, F., Allegrini, M.: 2001, *Phys. Rev. A*, **64**, 022719
- Kirova, T., Cinins, A., Efimov, D.K., Bruvelis, M., Miculis, K., Bezuglov, N.N., Auzinsh, M., Ryabtsev, I.I., Ekers, A.: 2017, *Phys. Rev. A*, **96**, 043421
- Landau, L., Lifshitz, E.: 1981, *Quantum Mechanics: Non-Relativistic Theory, Course of Theoretical Physics*, Butterworth-Heinemann: Oxford
- Metcalf, H.J., van der Straten, P.: 1999, *Laser Cooling and Trapping*, Springer New York: New York, NY
- Nikitin, E.E., Umanskii, S.Y.: 1984, *Theory of Slow Atomic Collisions*, Springer Berlin Heidelberg: Berlin, Heidelberg
- Porfido, N., Bezuglov, N.N., Bruvelis, M., Shayeganrad, G., Birindelli, S., Tantussi, F., Guerri, I., Viteau, M., Fioretti, A., Ciampini, D., Allegrini, M.,

- Comparat, D., Arimondo, E., Ekers, A., Fusoet, F.: 2015, *Phys. Rev. A*, **92**, 043408
- Rousseaux, B., Guérin, S., Vitanov, N.V.: 2013, *Phys. Rev. A*, **87**, 032328
- Schiff, L.I.: 1968, *Quantum Mechanics*, third ed., McGraw-Hill: New York
- Shore, B.W.: 2011, *Manipulating Quantum Structures Using Laser Pulses*, Cambridge University Press
- Shore, B.W.: 2017, *Adv. Opt. Photon*, **9**, 563
- Sobelman, I.I.: 1992, *Atomic Spectra and Radiative Transitions*, Springer
- Sydoryk, I., Bezuglov, N.N., Beterov, I.I., Miculis, K., Saks, E., Janovs, A., Spels, P., Ekers, A.: 2008, *Phys. Rev. A*, **77**, 042511
- Vitanov, N.V., Rangelov, A.A., Shore, B.W., Bergmann, K.: 2017, *Reviews of Modern Physics*, **89**, 015006